Selective area growth of AlGaN nanopyramid arrays on graphene by metal-organic vapor phase epitaxy

A. Mazid Munshi,[1] Dong-Chul Kim,[1] Carl Philip Heimdal,[1] Martin Heilmann,[2,a)] Silke H. Christiansen,[2,3] Per Erik Vullum,[4] Antonius T. J. van Helvoort,[5] and Helge Weman[1,6,b)]

[1]*CrayoNano AS, Sluppenvegen 6, 7037 Trondheim, Norway*
[2]*Max Planck Institute for the Science of Light, Staudtstrasse 2, 91058 Erlangen, Germany*
[3]*Helmholtz Centre Berlin for Materials and Energy, Hahn-Meitner Platz 1, 14109 Berlin, Germany*
[4]*SINTEF Industry, 7465 Trondheim, Norway*
[5]*Department of Physics, Norwegian University of Science and Technology (NTNU), 7491 Trondheim, Norway*
[6]*Department of Electronic Systems, Norwegian University of Science and Technology (NTNU), 7491 Trondheim, Norway*

(Received 14 August 2018; accepted 11 December 2018; published online 28 December 2018)

Wide-bandgap group III-nitride semiconductors are of special interest for applications in ultraviolet light emitting diodes, photodetectors, and lasers. However, epitaxial growth of high-quality III-nitride semiconductors on conventional single-crystalline substrates is challenging due to the lattice mismatch and differences in the thermal expansion coefficients. Recently, it has been shown that graphene, a two-dimensional material, can be used as a substrate for growing high-quality III–V semiconductors via quasi-van der Waals epitaxy and overcome the named challenges. Here, we report selective area growth of AlGaN nanopyramids on hole mask patterned single-layer graphene using metal-organic vapor phase epitaxy. The nanopyramid bases have a hexagonal shape with a very high nucleation yield. After subsequent AlGaN/GaN/AlGaN overgrowth on the six $\{10\bar{1}1\}$ semi-polar side facets of the nanopyramids, intense room-temperature cathodoluminescence emission is observed at 365 nm with whispering gallery-like modes. This work opens up a route for achieving III-nitride opto-electronic devices on graphene substrates in the ultraviolet region for future applications. https://doi.org/10.1063/1.5052054

III-Nitride ultraviolet light emitting diodes (UV LEDs) with the emission wavelength below 400 nm are expected to become extremely important for a variety of applications such as curing, sensing, food processing, and microbial disinfection of water and air.[1–3] Therefore, research and development has been intensified for growing high-quality epilayers within the AlGaN system with low dislocation density. However, epitaxial growth of these group III-nitrides is challenging due to the lack of suitable substrates.[4,5] Moreover, as the Al content is increased in the AlGaN epilayers to bring the wavelength into the deep UV region, needed for use in sterilization and disinfection applications, the dislocation density increases dramatically, further deteriorating device performance.[6] Modified growth processes[7,8] and expensive single-crystalline lattice matched substrates (e.g., AlN)[9] have been used to circumvent these issues, however, increasing the growth complexity and the device cost. Furthermore, the UV LEDs suffer from poor light extraction efficiency due to high substrate absorption, especially in the deep UV region (UVC), and large internal reflection at the planar substrate/air interface. In addition, conventional LEDs are grown on the polar $\{0001\}$ *c*-plane, resulting in the quantum-confined Stark effect which leads to further reduction of the device efficiency.[10,11] Therefore, applications of AlGaN-based UV LEDs are still limited, and energy-inefficient toxic mercury lamps with short operation life-times are mostly used in today's UVC technology.[2]

Nanostructured forms of semiconductors, such as nanowires and nanopyramids, can be grown almost defect-free due to their small foot-print and have received great attention in recent years for applications in solar cells,[12,13] LEDs,[14,15] and lasers[16] owing to their unique optoelectronic properties.[17] Moreover, the use of non-polar $\{10\bar{1}0\}$ and semi-polar $\{10\bar{1}1\}$ side facets for the active layers in III-nitride nanowires and nanopyramids makes the quantum-confined Stark effect less critical in LEDs.[18] In addition, theoretical calculations show that by manipulating the nanostructure size and separation, the light extraction efficiency of the LEDs can be drastically improved.[19]

Lately, epitaxial growth of III-nitride thin films[20,21] and nanostructures[22–25] on graphene has attracted great interest due to the excellent properties of graphene including high electrical and thermal conductivity, optical transparency (also in the deep UV regime), flexibility, and mechanical strength.[26] The absence of dangling bonds on the surface of graphene results in a weak quasi-van der Waals (vdWs) bonding between graphene and the grown semiconductor materials. Therefore, high quality materials can be grown epitaxially on graphene despite high lattice mismatch and differences in thermal expansion coefficients between graphene and the semiconductor. Moreover, for UV LED devices, graphene substrates may provide better thermal management[27] and can

a)Present address: Paul-Drude-Institut für Festkörperelektronik, Hausvogteiplatz 5-7, 10117 Berlin, Germany.
b)Author to whom correspondence should be addressed: helge.weman@ntnu.no.

also be used as electrodes for efficient light extraction owing to their unique transparency across the entire UV spectrum.[28] However, despite the potential of the III-nitride nanostructure/graphene hybrid heterostructure for UV LED applications, there are only a few literature reports, mainly regarding visible LEDs.[22,29] Here, we demonstrate positioned growth of AlGaN nanopyramid arrays with a very high yield on hole mask patterned graphene substrates using metal-organic vapor phase epitaxy (MOVPE). The room-temperature cathodoluminescence (CL) spectrum from nanopyramids shows near band edge GaN emission along with a defect peak. CL spectra from nanopyramids with overgrown AlGaN/GaN/AlGaN layers show intense near band edge GaN emission without any defect emission, together with whispering gallery-like modes.

Single-layer graphene, grown on a Cu-foil by chemical vapor deposition (CVD)[30,31] and transferred onto a 2″ native oxide covered Si(100) wafer by Graphenea, was used as the substrate. A schematic illustration for the preparation of the hole mask patterned graphene substrate and the growth of nanopyramid arrays is depicted in Fig. 1(a). The hole mask patterning was performed by electron-beam lithography (EBL). A combination of an amorphous aluminum oxide (∼10 nm) and silicon oxide (∼30 nm) stack was used as the mask layer. A square pattern with different hole sizes (60–270 nm) and pitches (hole-to-hole separation 0.7–5 μm), and a trigonal pattern with a 100 nm hole size and a 2 μm pitch were used for the growth of the nanopyramids. The hole size was controlled by the exposure time during the EBL process.

The nanopyramid growth was carried out in an Aixtron 200RF horizontal flow MOVPE reactor. Trimethylaluminum (TMAl), trimethylgallium (TMGa), and ammonia (NH_3) were used as precursors for Al, Ga, and N, respectively. The growth was carried out in a hydrogen (H_2) atmosphere at a reactor pressure of 75 Torr. Prior to the growth, the samples were thermally cleaned for 5 min in the presence of H_2 at 1200 °C, as measured by a thermocouple. The actual temperature on the surface of the substrate is expected to be about 100 °C lower than the measured temperature. After cleaning the substrate, a nitridation step was carried out using NH_3 for 10 min. Nitridation of graphene may result in an efficient nitrogen doping of graphene without creating structural defects.[32] However, it was found that AlGaN nanopyramids can also be grown without this nitridation step. After nitridation, an AlGaN nucleation layer was grown for 20 s with a gas phase Al ratio, TMAl/(TMAl + TMGa), of 0.23, followed by a second nitridation step for 2 min. During the growth of the nucleation layer, nanoscale AlGaN islands form on graphene, which can act as a seed and is critical for the subsequent growth of nanostructures.[25] The AlGaN nanopyramid growth was carried out for 150 s at 1150 °C with a gas phase Al ratio of 0.028. The TMAl, TMGa, and NH_3 flows were set to 2.6 μmol/min, 90 μmol/min, and 25 sccm, respectively, with an estimated V/III ratio of ∼12. In addition, silane was introduced during the growth to obtain n-type doping. After growth, the samples were cooled down to a substrate temperature of 500 °C in the presence of NH_3 and H_2. The morphological characterization of the nanopyramids was performed using a Hitachi S4800 scanning electron microscope (SEM) operated at 5 keV. To elucidate the optical properties, room-temperature CL measurements were carried out on the nanopyramids using a Tescan MIRA3 SEM operated at 5 keV and equipped with a Gatan MonoCL unit.

Representative SEM images of the AlGaN nanopyramid arrays are shown in Figs. 1(b) and 1(c) for the square pattern and in Fig. 1(d) for the trigonal pattern. The nanopyramids are found to have a very high nucleation yield (up to 99%) and good uniformity across the mask patterned area. A slight inhomogeneity in the size of the nanopyramids may be attributed to the statistical variation in the size and coverage of the seed layer in the holes. The nanopyramid bases have a

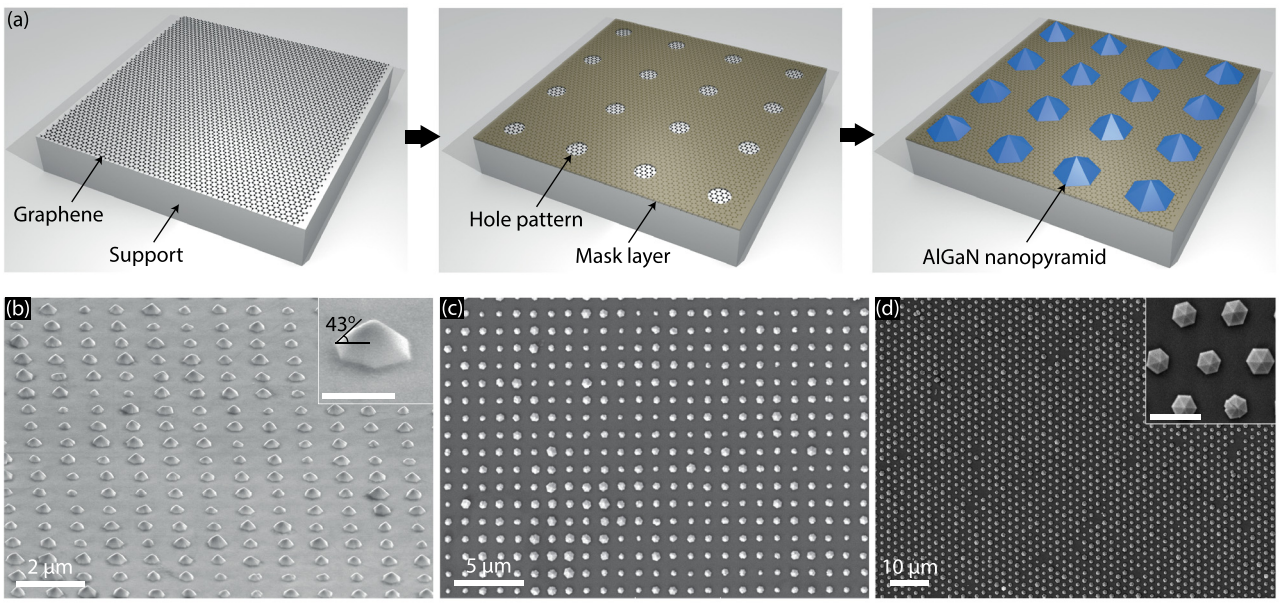

FIG. 1. (a) Schematic illustration of the hole mask patterning process and AlGaN nanopyramid growth on graphene. (b) and (c) Tilted- (b) and top-view (c) SEM images of AlGaN nanopyramid arrays on hole mask patterned graphene with a 1 μm pitch square pattern showing good uniformity and a very high nucleation yield. The scale bar in the inset of (b) is 400 nm. (d) Top-view SEM image of the AlGaN nanopyramid array on hole mask patterned graphene with a 2 μm pitch trigonal pattern. The scale bar in the inset is 2 μm.

hexagonal shape with six $\{10\bar{1}2\}$ side-facets, estimated by measuring a tilt angle of ~43° with the substrate [Fig. 1(b), inset]. The formation of the $\{10\bar{1}2\}$ side-facets is caused by the slow growth rate along the $\langle 10\bar{1}2\rangle$ directions due to the low NH_3 flow used for the nanopyramid growth.[33] In some holes, multiple AlGaN crystals started to grow on the AlGaN seed layer and eventually merged together, resulting in nanopyramids without well-defined facets.

The in-plane orientation of the pyramids was studied by top-view SEM images. In the present case, the Si substrate was covered with a native oxide on which polycrystalline graphene was transferred. Therefore, it is unlikely that there would be any epitaxial relation between GaN and the Si substrate. By close inspection of the pyramids in SEM, we do see that locally some of the pyramids have the same in-plane orientation in a particular region but are differently orientated from region-to-region. On the other hand, in some regions, the pyramids seem to have a similar in-plane orientation; however, if we see closely, they are mis-orientated from each other by a small (<5°) angle. Therefore, it is possible that the facet orientation in clusters of pyramids in some regions might be dictated by the polycrystalline graphene. Previously, in-plane orientation was reported for GaN nanowires on graphene by molecular beam epitaxy (MBE);[34] however, a random in-plane orientation was observed for GaN nanowires grown on graphene by MOVPE.[25] The apparent difference in the in-plane orientation of GaN grown by MBE and MOVPE could be associated with the much higher growth temperature for MOVPE as compared to MBE. Due to the high growth temperature and weak quasi-vdWs interaction, there may be a fluctuation in the orientation of the seed layer, resulting in the apparent random in-plane orientation of the GaN nanostructures during the subsequent growth.

Figure 2(a) shows the room-temperature CL spectrum taken from a single nanopyramid with an emission peak at 366 nm, together with a strong defect luminescence at around 550 nm. The 366 nm peak corresponds to the GaN band-edge emission, and no emission related to AlGaN was observed despite that 2.8% Al in the gas phase was used during growth. This indicates sub-optimal growth conditions with a reduced material quality, as evident also by the broad band-edge emission and strong defect luminescence, possibly caused by the use of low NH_3 and high silane flows.

The nanopyramids are overgrown with AlGaN/GaN/AlGaN with 20% Al in the gas phase, using a high NH_3 flow at the same reactor pressure and temperature as used for the nanopyramid growth. The TMAl, TMGa, and NH_3 flows were set to 11.5 μmol/min, 45 μmol/min, and 1500 sccm, respectively. The growth duration of the AlGaN/GaN/AlGaN heterostructure was set to 15, 1, and 15 min, respectively. The total thickness of the shell in the regrown core-shell pyramid using TEM was estimated to be 300 nm. Figure 2(b) shows the CL spectrum taken from a single pyramid after the overgrowth. Figure 2(c) shows the top-view SEM image of the overgrown pyramid from where the CL spectrum in Fig. 2(b) was taken. Figure 2(d) shows the panchromatic CL intensity mapping of the same pyramid. The CL spectrum from the overgrown pyramid [Fig. 2(b)] shows intense near band edge emission centered at 363 nm, with multiple peaks towards the longer

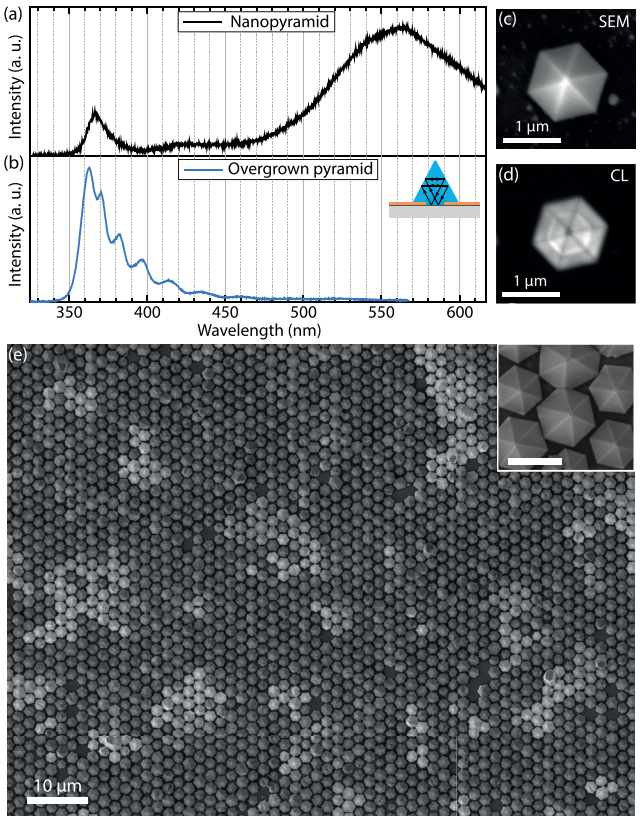

FIG. 2. (a) and (b) Room-temperature CL spectra obtained from a single pyramid from the same sample in Figs. 1(b) and 1(c) and from a single AlGaN/GaN/AlGaN overgrown pyramid. The inset in (b) is the schematic illustration of the whispering gallery mode formation. (c) and (d) SEM image and panchromatic CL intensity mapping of the same pyramid from which the CL spectrum in (b) was acquired. (e) Top-view SEM image of overgrown pyramid arrays on the same sample shown in Fig. 1(d). The inset shows the magnified view of the same sample. The scale bar in the inset is 2 μm.

wavelength shoulder. It is observed that that the spacing of the modes scales inversely with the size of the pyramids. No defect related luminescence was observed from the overgrown pyramid. The multiple CL peaks are believed to be whispering gallery-like modes inside the pyramid.[35] This superior optical quality of the overgrown pyramids may be caused by the use of high NH_3 flow leading to the formation of a very regular hexagonal shape with smooth side-facets. Figure 2(e) shows an overview SEM image of the overgrown pyramid arrays in a 1 μm pitch trigonal pattern. It can be seen that the overgrown pyramids have a very high yield and are well-developed facets.

Structural and compositional features of the pyramids were studied by cross-sectional TEM using a double Cs-corrected JEOL ARM 200F TEM/STEM operated at 80 keV. The TEM lamella was prepared by focused ion beam (FIB) using an FEI Helios G4 UX. C layers (e-beam assisted deposition for the first layer) were deposited on top of the region of interest as a protection during the Ga^+ ion-beam thinning. The coarse thinning was performed with a 30 kV acceleration voltage for the Ga^+ ions. Final thinning was done at 5 and 2 kV. Figure 3(a) shows a bright-field (BF) TEM image with the electron beam parallel to $[1\bar{2}10]$ orientation. It can be noticed that during overgrowth, the $\{10\bar{1}1\}$ side-facets of the pyramids have become stable due to the high NH_3 flow

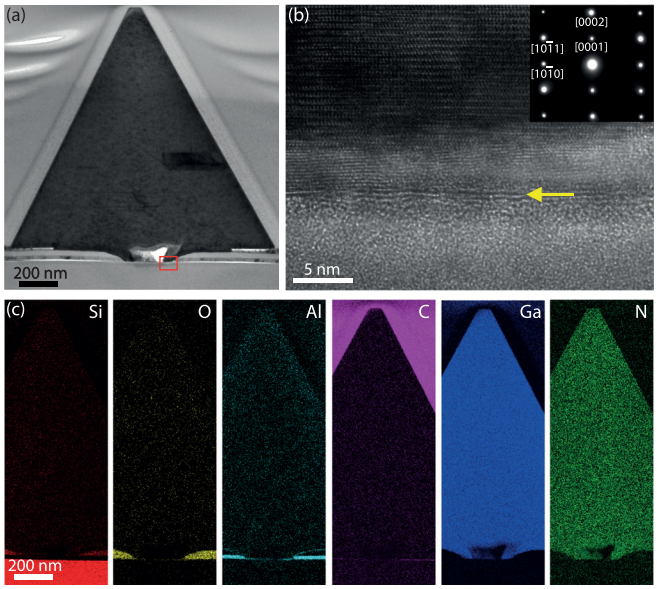

FIG. 3. (a) BF TEM image of a pyramid with electron beam parallel to the $[1\bar{2}10]$ direction. (b) HRTEM image of the pyramid/graphene/Si support interface marked in the red rectangular region in (a). Weak observation of carbon from the single layer graphene is indicated by a yellow arrow. The inset shows the $[1\bar{2}10]$ diffraction pattern from the pyramid in (a). (c) Elemental maps of the pyramid in (a). EELS was used to make the Si, O, C, and N maps, whereas EDS was used to make the Al and Ga maps.

and prolonged growth time,[33] estimated by measuring an angle of ∼62° with the substrate [Fig. 3(a)]. A cavity region at the center of the pyramid can be observed in Fig. 3(a). The AlGaN nucleation layer is likely to first nucleate on graphene at the edge of the holes in the mask. Subsequently, nanopyramids start to grow from this nucleation layer. This might leave a cavity above the graphene at the center of the hole in the mask. The inset in Fig. 3(b) shows a high-resolution (HR) TEM image of the pyramid/graphene/Si support interface from the marked region in Fig. 3(a). The inset of Fig. 3(b) shows the $[1\bar{2}10]$ zone axis diffraction pattern from the pyramid depicting a wurtzite crystal structure with the growth direction along the *c*-axis, as expected. At the bottom of the pyramid (i.e., at the interface between the pyramid and the Si support with a native silicon oxide), there is a layer with slightly different contrast indicated by the yellow arrow in Fig. 3(b). This is interpreted as the single graphene layer. On top of it, there is a 3–4 nm thick Al-rich AlGaN nucleation layer followed by the pyramid with no detectable amounts of Al.

Compositional analysis was performed by X-ray energy dispersive spectroscopy (EDS) and electron energy loss spectroscopy (EELS) in the scanning TEM (STEM) mode on the pyramid in Fig. 3(a). Elemental maps extracted from EELS (Si, O, C, N) and EDS (Al, Ga) are shown in Fig. 3(c). A very thin layer of carbon from graphene is observed at the interface between the pyramid and the Si support. There is hardly any Al in the pyramid, except a small amount at the very top, and significant amount at the bottom. We attribute this low Al incorporation in the pyramid to the parasitic reaction[36] especially due the use of a horizontal flow MOVPE and a longer diffusion length of Ga species as compared to Al.[37] The longer diffusion length of Ga makes Ga supply more effective as compared to Al at the bottom part of the pyramid, resulting in a lower Al composition. But on the top part of the pyramid, Ga tends to escape due to its long diffusion length, resulting in a higher Al composition. We expect that the incorporation of Al in the structure can be achieved by modified growth techniques, e.g., pulsed-growth technique or using vertical flow MOVPE reactors.

In conclusion, AlGaN nanopyramid arrays have been grown on hole mask patterned single-layer graphene using MOVPE. The nanopyramids were found to have a hexagonal shape and a very high nucleation yield. Subsequently, the nanopyramids were overgrown with AlGaN/GaN/AlGaN on the six semi-polar side facets. Room-temperature CL from the overgrown nanopyramids shows intense near band edge emission at 363 nm, together with whispering gallery-like modes. The low Al content in the AlGaN pyramids was corroborated by TEM, suggesting the need for further optimization of the MOVPE growth conditions. The positioned nanopyramid arrays reported here lays a foundation for growing AlGaN-based nanopyramid and nanowire arrays on graphene for future UV LEDs.

The Research Council of Norway is acknowledged for the support from the EUROSTARS program of EUREKA and the European Union (Grant No. 264206), the NANO2021 program of the Research Council of Norway (Grant No. 259553), and the Norwegian Micro- and Nano-Fabrication Facility, NorFab (Grant No. 245963). The TEM work was carried out on NORTEM infrastructure (Grant No. 197405), TEM Gemini Centre, Norwegian University of Science and Technology (NTNU), Norway. The German Research Foundation (DFG) is acknowledged for the support within the research project "Dynamics and Interactions of Semiconductor Nanowires for Optoelectronics" (FOR1616).

[1]A. Khan, K. Balakrishnan, and T. Katona, Nat. Photonics **2**, 77 (2008).
[2]Y. Muramoto, M. Kimura, and S. Nouda, Semicond. Sci. Technol. **29**, 084004 (2014).
[3]M. Kneissl, "A brief review of III-nitride UV emitter technologies and their applications," in *III-Nitride Ultraviolet Emitters: Technology and Applications*, edited by M. Kneissl and J. Rass (Springer International Publishing, Cham, 2016), p. 1.
[4]P. Kung and M. Razeghi, Opto-Electron. Rev. **8**, 201 (2000), available at https://www.scholars.northwestern.edu/en/publications/iii-nitride-wide-bandgap-semiconductors-a-survey-of-the-current-s.
[5]D. Zhu, D. J. Wallis, and C. J. Humphreys, Rep. Prog. Phys. **76**, 106501 (2013).
[6]M. Kneissl, T. Kolbe, C. Chua, V. Kueller, N. Lobo, J. Stellmach, A. Knauer, H. Rodriguez, S. Einfeldt, Z. Yang, N. M. Johnson, and M. Weyers, Semicond. Sci. Technol. **26**, 014036 (2011).
[7]J. Zhang, X. Hu, A. Lunev, J. Deng, Y. Bilenko, T. M. Katona, M. S. Shur, R. Gaska, and M. A. Khan, Jpn. J. Appl. Phys. **44**, 7250 (2005).
[8]H. Hirayama, T. Yatabe, N. Noguchi, T. Ohashi, and N. Kamata, Appl. Phys. Lett. **91**, 071901 (2007).
[9]M. Kneissl, Z. Yang, M. Teepe, C. Knollenberg, O. Schmidt, P. Kiesel, N. M. Johnson, S. Schujman, and L. J. Schowalter, J. Appl. Phys. **101**, 123103 (2007).
[10]T. Deguchi, K. Sekiguchi, A. Nakamura, T. Sota, R. Matsuo, S. Chichibu, and S. Nakamura, Jpn. J. Appl. Phys. Part II **38**, L914 (1999).
[11]P. Lefebvre, B. Gil, J. Allègre, H. Mathieu, N. Grandjean, M. Leroux, J. Massies, and P. Bigenwald, MRS Proc. **537**, G3.69 (1998).
[12]Y. Dong, B. Tian, T. J. Kempa, and C. M. Lieber, Nano Lett. **9**, 2183 (2009).
[13]J. J. Wierer, Jr., Q. Li, D. D. Koleske, S. R. Lee, and G. T. Wang, Nanotechnology **23**, 194007 (2012).

[14]J. H. Choi, A. Zoulkarneev, S. I. Kim, C. W. Baik, M. H. Yang, S. S. Park, H. Suh, U. J. Kim, H. Bin Son, J. S. Lee, M. Kim, J. M. Kim, and K. Kim, Nat. Photonics **5**, 763 (2011).
[15]S. Li and A. Waag, J. Appl. Phys. **111**, 071101 (2012).
[16]K. H. Li, X. Liu, Q. Wang, S. Zhao, and Z. Mi, Nat. Nanotechnol. **10**, 140 (2015).
[17]M. Mandl, X. Wang, T. Schimpke, C. Kölper, M. Binder, J. Ledig, A. Waag, X. Kong, A. Trampert, F. Bertram, J. Christen, F. Barbagini, E. Calleja, and M. Strassburg, Phys. Status Solidi RRL **7**, 800 (2013).
[18]Y.-R. Wu, C. Y. Huang, Y. Zhao, and J. Speck, "Nonpolar and semipolar LEDs," in *Nitride Semiconductor Light-Emitting Diodes (LEDs)*, 2nd ed., edited by J. J. Huang, H. C. Kuo, and S. C. Shen (Woodhead Publishing, 2018), p. 273.
[19]M. Djavid and Z. Mi, Appl. Phys. Lett. **108**, 051102 (2016).
[20]J. Kim, C. Bayram, H. Park, C.-W. Cheng, C. Dimitrakopoulos, J. A. Ott, K. B. Reuter, S. W. Bedell, and D. K. Sadana, Nat. Commun. **5**, 4836 (2014).
[21]Y. Xu, B. Cao, Z. Li, D. Cai, Y. Zhang, G. Ren, J. Wang, L. Shi, C. Wang, and K. Xu, ACS Appl. Mater. Interfaces **9**, 44001 (2017).
[22]K. Chung, H. Beak, Y. Tchoe, H. Oh, H. Yoo, M. Kim, and G.-C. Yi, APL Mater. **2**, 092512 (2014).
[23]H. Hayashi, Y. Konno, and K. Kishino, Nanotechnology **27**, 055302 (2016).
[24]S. Kang, A. Mandal, J. H. Chu, J.-H. Park, S.-Y. Kwon, and C.-R. Lee, Sci. Rep. **5**, 10808 (2015).
[25]M. Heilmann, A. M. Munshi, G. Sarau, M. Göbelt, C. Tessarek, V. T. Fauske, A. T. J. van Helvoort, J. Yang, M. Latzel, B. Hoffmann, G. Conibeer, H. Weman, and S. Christiansen, Nano Lett. **16**, 3524 (2016).
[26]A. K. Geim and K. S. Novoselov, Nat. Mater. **6**, 183 (2007).
[27]Z. Yan, G. Liu, J. M. Khan, and A. A. Balandin, Nat. Commun. **3**, 827 (2012).
[28]F. Bonaccorso, Z. Sun, T. Hasan, and A. C. Ferrari, Nat. Photonics **4**, 611 (2010).
[29]J. Kang, Z. Li, H. Li, Z. Liu, X. Li, X. Yi, P. Ma, H. Zhu, and G. Wang, Appl. Phys. Express **6**, 072102 (2013).
[30]X. Li, W. Cai, J. An, S. Kim, J. Nah, D. Yang, R. Piner, A. Velamakanni, I. Jung, E. Tutuc, S. K. Banerjee, L. Colombo, and R. S. Ruoff, Science **324**, 1312 (2009).
[31]T. Araki, S. Uchimura, J. Sakaguchi, Y. Nanishi, T. Fujishima, A. Hsu, K. K. Kim, T. Palacios, A. Pesquera, A. Centeno, and A. Zurutuza, Appl. Phys. Express **7**, 071001 (2014).
[32]G. Sarau, M. Heilmann, M. Bashouti, M. Latzel, C. Tessarek, and S. Christiansen, ACS Appl. Mater. Interfaces **9**, 10003 (2017).
[33]A. Lundskog, U. Forsberg, P. O. Holtz, and E. Janzén, Cryst. Growth Des. **12**, 5491 (2012).
[34]V. Kumaresan, L. Largeau, A. Madouri, F. Glas, H. Zhang, F. Oehler, A. Cavanna, A. Babichev, L. Travers, N. Gogneau, M. Tchernycheva, and J.-C. Harmand, Nano Lett. **16**, 4895 (2016).
[35]H. X. Jiang, J. Y. Lin, K. C. Zeng, and W. Yang, Appl. Phys. Lett. **75**, 763 (1999).
[36]V. Jindal, J. R. Grandusky, N. Tripathi, F. Shahedipour-Sandvik, S. LeBoeuf, J. Balch, and T. Tolliver, J. Mater. Res. **22**, 838 (2007).
[37]T. Kato, Y. Honda, Y. Kawaguchi, M. Yamaguchi, and N. Sawaki, Jpn. J. Appl. Phys. Part I **40**, 1896 (2001).